IEEE Access
Multidisciplinary | Rapid Review | Open Access Journal

Received 5 December 2023, accepted 24 December 2023, date of publication 28 December 2023,
date of current version 9 January 2024.

Digital Object Identifier 10.1109/ACCESS.2023.3347780

RESEARCH ARTICLE

Prognostics and Health Management Using Nonlinear Cumulative Damage Model for Electronic Devices Under Variable Loading

SUYEON LEE, SEUNGIL PARK, AND CHANGWOON HAN
Department of Mechanical Engineering, The State University of New York, Korea, Incheon 21985, Republic of Korea
Corresponding author: Changwoon Han (changwoon.han@sunykorea.ac.kr)

This work was supported in part by the National Research Foundation of Republic of Korea under Grant 2021R1F1A-1052595, and in part by the Korea Evaluation Institute of Industrial Technology of Republic of Korea under Grant 20017488.

ABSTRACT This paper explores nonlinear cumulative damage models applied to Prognostics and Health Management in electronic systems, with a focus on solder joint reliability under variable vibrations. Several cumulative damage models, including the total strain energy density model, are investigated to address the limitation of Miner's rule. The State-of-Damage (SoD) concept is introduced as a pivotal metric for evaluating Prognostics and Health Management performance within each model. A novel SoD definition with a scale factor is proposed to balance linearity and exponential behavior, meeting the demands of real-time monitoring. Furthermore, by calculating Remaining Useful Life (RUL) using the SoD metric, the RUL predictions from Miner's rule and total strain energy density model with the scale factor are compared. The results reveal that the total strain energy density model, enhanced with the scale factor, outperforms Miner's rule in accurately predicting SoD and RUL. This study advances Prognostics and Health Management methodologies by introducing an innovative SoD concept with a scale factor, resulting in enhanced accuracy for both SoD and RUL predictions. This innovation holds the potential for more reliable electronic systems under variable loading conditions.

INDEX TERMS Cumulative damage model, prognostics and health management, remaining useful life, state-of-damage, total strain energy density model.

NOMENCLATURE

A, B, C, D	Material constants.
a	Crack length.
b, c	Fatigue strength exponents.
f_1	First natural frequency of the system.
m_k	Cumulative number of applied cyclic loading in an equivalent scale at the load step k.
$m_{k-1@k}$	Equivalent m_{k-1} at the load step k.
N_k	Number of failure cyclic loading in the load step k.
N_e	Number of cycles for the endurance limit.
n_k	numbe r of applied cyclic loading in the load step k.
n_{RUL}	The remaining number of cycles to failure at a stress level.
SoD_M	State-of-Damage defined by Miner's approach.
SoD_S	State-of-Damage defined by slope comparison.
SoD_λ	State-of-Damage defined by scale factor.
s_k	Normalized stress at the load step k.
s_u	Normalized stress of the ultimate stress.
s_e	Normalized stress of the endurance limit stress.
U	Normalized energy density per cycle.
U_k	Normalized energy density per cycle at the load step k.

The associate editor coordinating the review of this manuscript and approving it for publication was Jiajie Fan.

W	Total strain energy density per cycle.
W^p	Plastic strain energy density per cycle.
W^e	Elastic strain energy density per cycle.
W_u	Total strain energy density at the ultimate stress.
α, β	Material constants.
λ	Scale factor.
σ_e	Endurance limit stress.
σ_k	Stress at the load step k.
$\bar{\sigma_k}$	Mean tensile stress at the load step k.
σ_{Mk}	Maximum tensile stress at the load step k.
σ_u	Ultimate stress.
γ	Strain.

TABLE 1. Selected CDMs alternating Miner's rule from reference [16].

Category	Selected model	Model expression
Curve damage model	Damage curve approach	$\left(\frac{n_1}{N_1}\right)^{\frac{N_1}{N_2}^{0.4}} + \frac{n_2}{N_2} = 1$
Crack growth damage model	Short crack theory	$\frac{da}{dN} = A(\Delta\gamma)^{\alpha}(d-a)$ or $= B(\Delta\gamma)^{\beta}a - D$
Modifying damage model	Hashin-Rotem (HR) model	$\left(\frac{n_1}{N_1}\right)^{\frac{\log s_2}{\log s_1}} + \frac{n_2}{N_2} = 1$
Energy-based damage model	Total Strain energy density (TS) model	$\left(\frac{n_1}{N_1}\right)^{\frac{\log(N_2/N_e)}{\log(N_1/N_e)}} + \frac{n_2}{N_2} = 1$
Continuum damage model	Lemaitre-Chaboche model	$\left(\frac{n_1}{N_1}\right)^{\frac{\sigma_{M2}-\sigma_1(\overline{\sigma_2})}{\sigma_{M1}-\sigma_1(\overline{\sigma_1})}\frac{\sigma_u-\sigma_{M1}}{\sigma_u-\sigma_{M2}}} + \frac{n_2}{N_2} = 1$

I. INTRODUCTION

Electronics have become indispensable parts of modern life, and the mobility industry is no exception. The main trends of future mobility industry, such as Autonomous, Connective, Electric, and Sharing (ACES) technologies, are transforming the driving system from a mechanical to an electrical/software-based system [1]. Vehicles are exposed to harsh environments such as temperature variations and vibrations caused by rough road conditions. Temperature, vibration as well as humidity and dust, have mainly been considered as conventional causes of vehicle failure [2], [3].

With the increasing adoption of Autonomous driving and Sharing vehicles in the future mobility, it is anticipated that the milage of a vehicle over a certain period will increase, and accordingly, the impact of variable vibration to the failure of a vehicle will be accelerated. Furthermore, as vehicle mileage increases, the failure mode of electronic equipment will expand to the domain of wear-out failure beyond infant or random failures. Therefore, it is crucial to develop effective maintenance techniques and application methods that can accurately predict and prevent failures of electronic systems in vehicles caused by variable vibration conditions. These advancements will ensure the safe and reliable operation of electronic devices in the future of mobility, addressing the challenges posed by vibrations.

Prognostics and Health Management (PHM) technology has found widespread adoption in many industries that require high reliability and safety. It facilitates real-time health assessment of a system in its current operating state and predicts its future state based on current information [4]. However, compared to PHM for mechanical systems, the development of PHM for electronic systems has faced more challenges [5]. This is primarily due to the unique attributes of electronic systems, such as the absence of degrading but abrupt changing data signals in systems [6]. Despite continuous research and development efforts since its introduction, PHM for electronics is still limited to the stage of applied technology, as indicated by a PHM technology development roadmap [7].

As a method to implement PHM in electronics, two approaches for electronic PHM have been identified: Monitoring Precursor Failure (MPF) and Monitoring Environmental Stress (MES) methods [8], [9]. MPF involves predicting remaining life based on a failure-related electronic signal or failure precursor. It is an efficient method for predicting remaining life by directly measuring the failure precursor from the system. However, MPF may not be always applicable to electronic components that lack precursors or exhibit abrupt changes in data signals, such as sudden failure [10]. Moreover, practical applications may have limitations, as not all failure precursor parameters can be easily measured [11].

In contrast, MES aims to predict the current status of health and forecast Remaining Useful Life (RUL) by monitoring environmental stress such as temperature, vibration, humidity, and voltage, which can cause physical or chemical damage to components or systems [12]. This method requires the use of Life Prediction Model (LPM), which establishes the relationship between constant environmental stress and the component's life, such as an S-N curve. Additionally, to implement LPM on PHM under variable loading in real conditions, a Cumulative Damage Model (CDM) is required. The CDM, such as Miner's rule, can predict the current health status using a concept of damage. To predict the RUL of electronic components under a variable loading condition, both LPM and CDM are necessary.

The purpose of this study is on improving the MES method by advancing the CDM to enhance the accuracy of prediction in PHM for electronics under variable loading conditions. Miner's rule, a representative CDM in MES, is widely acknowledged for its effectiveness in implementing on PHM scheme. However, its limitations are also well-known, such as the independence of load level and load sequence in predictions, leading to discrepancies and inaccuracies [13], [14]. To address this, we have revisited the alternative CDMs and the damages defined in the models. Subsequently, we have identified some problems in implementing these concepts with the framework of PHM and proposed a novel definition of damage in CDMs, which can be effectively implemented in the PHM framework and predicting the RULs. The proposition has been proved with a set of variable vibration experiment conducted using actual

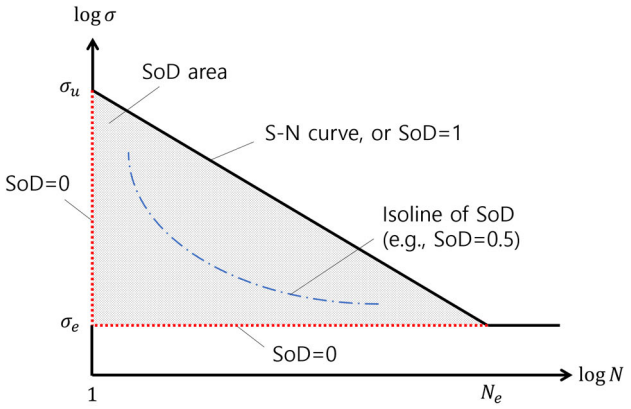

FIGURE 1. Illustration of SoD concept on a life model.

mobility field profile for an electronic system. This approach will provide a valuable tool for monitoring the health of electronic components under variable vibration conditions, contributing to improved maintenance strategies, and prolonging their operational lifespan in the mobility industry by enhancing the accuracy of predicting the damage and RUL of electronic components.

II. SELECTION OF CDMs

Since the introduction of Miner's rule, numerous alternative CDMs have been researched and suggested to address the inherent issues in the rule, as documented in various review papers [15], [16], [17]. In a comprehensive study by Fatemi and Yang [16], over 50 CDMs were analyzed and classified into several categories. Based on the study, we have researched and selected models that have the potential to replace Miner's rule. The selection criteria were based on the popularity of the models, measured by the number of citations within each category. The results are summarized in Table 1. Note that all the models except the short crack theory are nonlinear CDMs that follow an exponential expression of the damage curve approach.

Among the models, the damage curve approach was developed for the application to steel material, employing an exponent of 0.4 in the expression. To extend its application to other materials, it is imperative to derive the appropriate exponent for each specific material through experimentation. Furthermore, the short crack theory and the Lemaitre-Chaboche model were grounded on the fracture mechanics, aiming to elucidate the physical behavior of crack initiation and propagation during damage evolution. However, their utilization necessitates an elastic-plastic analysis to quantify the crack behavior and a deeper comprehension of crack initiation, as stated by Miller [18]. Additionally, within these models, damage was evaluated based on the length of the crack, yet the criteria for failure remain unclear, making it difficult to assess the remaining life of electronics. Consequently, in this study, the Hashin-Rotem (HR) model and the Total Strain energy density (TS) model were selected as candidates to replace Miner's rule.

III. DEFINITION OF STATE-OF-DAMAGE IN CDMs

As all the expressions of CDMs in the Table 1 suggest, they were originally invented to tell the failure or not (1 or not) at a certain load step of failure. To implement the CDMs in the PHM, the concept of State-of-Damage (SoD) needs to be introduced. SoD is a conceptual metric that accumulates from zero to one within a material until it reaches failure when subjected to a series of stresses. It plays a crucial role in evaluating the health status of the material and calculating its RUL.

Mathematically, there are various ways to define SoD. A conceptual representation of the SoD definition is presented on a log-log scale S-N curve in Fig. 1. The line where SoD equals one corresponds to the S-N curve itself, indicating the point of failure. In addition, two lines where SoD equals zero, representing no damage accumulated, can be identified. These lines run along $N = 1$ and $\sigma = \sigma_e$, as depicted in Fig. 1. The triangular region enclosed by SoD $= 0$ and SoD $= 1$ can serve as a framework in defining SoD. Within the region, lines can be drawn where the SoD level remains constant, leading to the concept of isolines of SoD. In this study, we adopted the concept of straight isolines of SoD to establish a mathematical definition of SoD. It is worth noting that the concept of isolines of damage under S-N curve diagram was originally introduced by Subramanyan in his study [19].

A. STATE-OF-DAMAGE IN MINER'S RULE

When a material undergoes a sequence of load steps involving different stress levels, Miner [20] introduced a method to estimate the SoD (SoD_M) experienced by the material. In this rule, when the total k load steps are applied to the material, SoD_M is calculated as the sum of the ratios of the number of applied cycling loading in each load step (n_i) to the material's fatigue life obtained from the S-N curve under that specific load step (N_i). Mathematically, the Miner's SoD can be expressed as:

$$SoD_M = \sum_{i=1}^{k} \frac{n_i}{N_i}. \tag{1}$$

When SoD_M reaches a value of one, it indicates that the material has accumulated sufficient damage to reach its end of life or failure point.

In this study, an alternative representation of Miner's rule is employed to represent it graphically, as follows:

$$SoD_M = \frac{m_k}{N_k}. \tag{2}$$

Here, m_k is the cumulative number of applied cyclic loading in an equivalent scale at the load step k, defined as

$$m_1 = n_1 \text{ when } k = 1, \tag{3a}$$
$$m_k = n_k + m_{k-1@k}, \text{ when } k \neq 1. \tag{3b}$$

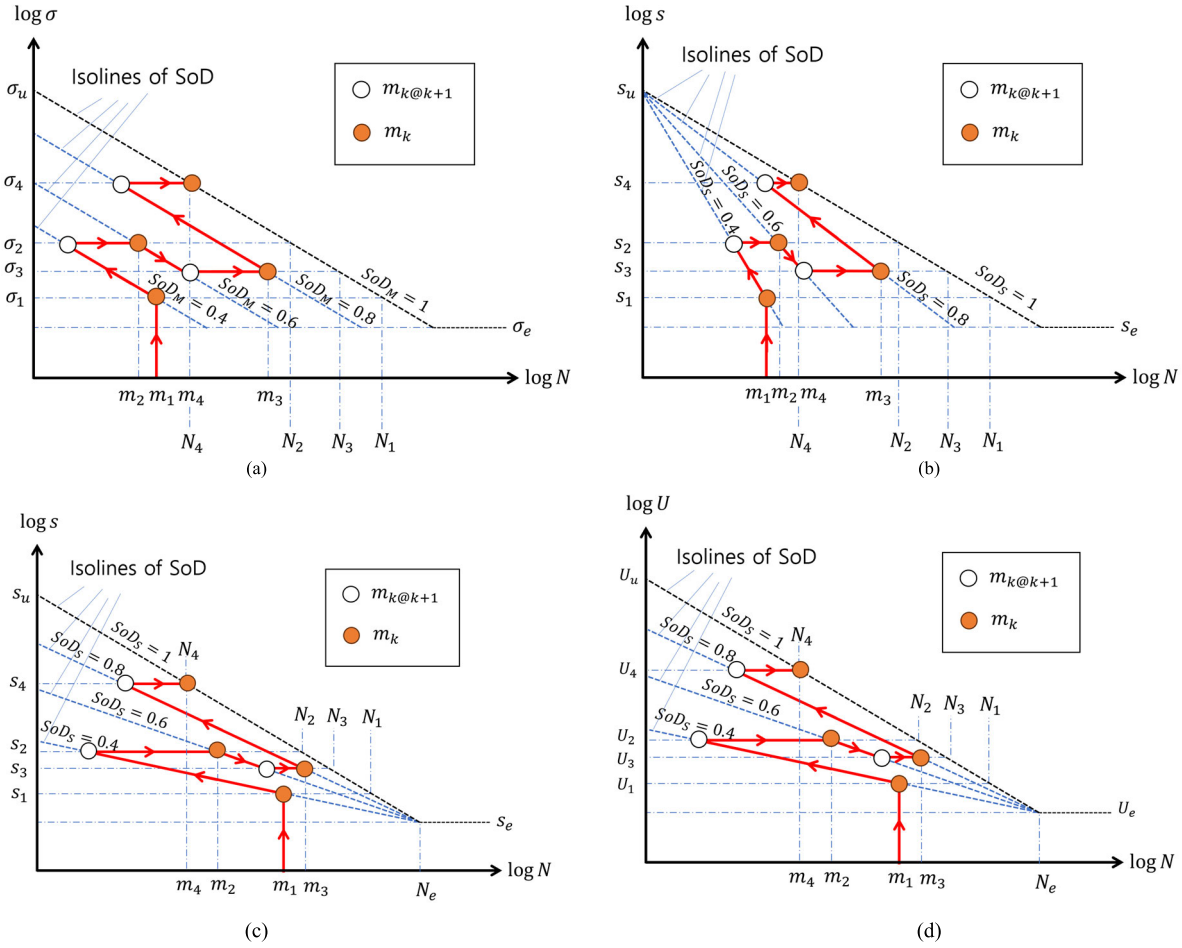

FIGURE 2. Illustration of isolines and growth of SoD in (a) Miner's rule, (b) HR-Su model, (c) HR-Se model, and (d) TS model.

where $m_{k-1@k}$ denotes an equivalent m_{k-1} at the load step k, defined as

$$m_{k-1@k} = \frac{N_k}{N_{k-1}} m_{k-1} \tag{4}$$

It can be easily proved that (1) and (2) are equivalent. Moreover, by taking the logarithm of (4) and dividing it by stress ratio, it can be written as

$$\frac{\log m_{k-1@k} - \log m_{k-1}}{\log \sigma_k - \log \sigma_{k-1}} = \frac{\log N_k - \log N_{k-1}}{\log \sigma_k - \log \sigma_{k-1}}. \tag{5}$$

This equation suggests the concept of isolines of SoD parallel to S-N curve in the log-log scale. The growth of damage represented by (2) in a variable loading can be visualized in the S-N curve diagram, confirming the concept of isolines of SoD where the level of SoD is equivalent. In Figure 2(a), an illustration of the isolines and the growth of SoD with the Miner's rule is shown. In this example, we consider a sequence of fatigue stresses comprising four steps in the temporal sequences: σ_1, σ_2, σ_3, and σ_4, causing SoD growth on the material at scales of 0.4, 0.6, 0.8, and 1.0, respectively. The magnitudes of the stresses are randomly distributed. The stress levels and resulting SoDs determine the coordinates of points of m_1 through m_4 from (2) as depicted in Fig. 2(a). Additionally, equation (4) facilitates the determination of points $m_{1@2}$, $m_{2@3}$, and $m_{3@4}$, contributing to the formation of SoD isolines with values $SoD_M = 0.4$, 0.6, 0.8, and 1.0, which run in parallel to the S-N curve as represented in Fig. 2(a). Note that the line of $SoD_M = 1.0$ coincides with the S-N curve itself.

B. STATE-OF-DAMAGE IN HR MODELS

In Figure 2(a), the concept of Miner's rule is visually explained through isolines of SoD that run parallel to the S-N curve. However, this depiction also highlights some limitations of Miner's rule from other perspectives. Firstly, Miner's rule falls short in capturing the impact of load sequencing, such as transitions from high-to-low and low-to-high load changes. Moreover, the situation where $N = 1$ raises a challenge, allowing for the selection of multiple stresses to contribute to SoD. This situation mirrors the case where the stress level aligns with $\sigma = \sigma_e$. In order to address these concerns, Hashin and Rotem introduced the ultimate strength (HR-Su) and endurance limit (HR-Se) models as viable alternatives to Miner's rule [21], [22].

An illustrative example of HR-Su model is shown in Fig. 2(b), following the same setup as in Fig. 2(a). In this figure, stress is normalized as $s_k = \sigma_k/\sigma_u$ to facilitate the mathematical formulation of isolines of SoD, and the S-N curve is modeled as $\log s_k = \Gamma \log N_k$ with the exponential factor Γ for the log-log scale. Notably, Figure 2(b) has the isolines of SoD intersecting at the ultimate strength (s_u), satisfying the requirement of $D = 1$ when s_u is applied. In this context, the mathematical representation of isolines of SoD can be expressed as follows:

$$\frac{\log m_{k-1@k} - \log 1}{\log s_k - \log s_u} = \frac{\log m_{k-1} - \log 1}{\log s_{k-1} - \log s_u} \quad \text{or } m_{k-1@k} = m_{k-1}^{\frac{\log s_k}{\log s_{k-1}}}, \tag{6}$$

which is equivalent to (4) and (5) in the Miner's rule.

In the HR-Su model, the SoD can be defined in two ways. Firstly, by following the way of Miner's rule or (2):

$$SoD_M\ |_{HR\_Su} = \frac{m_k}{N_k} = \frac{n_k + m_{k-1@k}}{N_k} = \frac{n_k}{N_k} + \left(\frac{m_{k-1}}{N_{k-1}}\right)^{\frac{\log s_k}{\log s_{k-1}}} \tag{7}$$

It can be further expressed as:

$$SoD_M\ |_{HR\_Su} = \left(\left(\left(\frac{n_1}{N_1}\right)^{\frac{\log s_2}{\log s_1}} + \frac{n_2}{N_2}\right)^{\frac{\log s_3}{\log s_2}} \cdots \frac{n_{k-1}}{N_{k-1}}\right)^{\frac{\log s_k}{\log s_{k-1}}} + \frac{n_k}{N_k}, \tag{8}$$

which represents the original definition of model in Hashin and Rotem study [22].

Secondly, by utilizing the concept of the isolines of SoD, SoD can be also defined through the concept of relative slope as follows:

$$SoD_S\ |_{HR\_Su} = min\left(\frac{slope\ (N_k)}{slope\ (m_k)}, \frac{slope\ (m_k)}{slope\ (N_k)}\right), \tag{9}$$

where $slope(i)$ represents the slope of SoD isoline at the intersection point i. For the HR-Su model, SoD_S will be:

$$SoD_S\ |_{HR\_Su} = \frac{\log s_k}{\log N_k} / \frac{\log s_k}{\log m_k} = \frac{\log m_k}{\log N_k}. \tag{10}$$

The relation between $SoD_S\ |_{HR\_Su}$ and $SoD_M\ |_{HR\_Su}$ can be derived as:

$$SoD_S\ |_{HR\_Su} = \frac{\log\ (SoD_M\ |_{HR\_Su})}{\log\ (N_k)} + 1 \tag{11}$$

The comparison of SoD_S and SoD_M for the implementation in PHM is discussed in the Section V.

The HR-Su model addresses the problem of the Miner's rule when $N = 1$, but it does not resolve the issue at the endurance limit (s_e). It can be addressed by considering the isolines of SoD from the s_e, following a similar approach to HR-Su model as represented in Fig. 2(c). The mathematical formulation of the isolines of SoD follows:

$$\frac{\log m_{k-1@k} - \log N_e}{\log s_k - \log s_e} = \frac{\log m_{k-1} - \log N_e}{\log s_{k-1} - \log s_e} \quad \text{or } \frac{m_{k-1@k}}{N_e} = \left(\frac{m_{k-1}}{N_e}\right)^{\frac{\log (s_k/s_e)}{\log (s_{k-1}/s_e)}}. \tag{12}$$

Using this relation, SoD can be also defined by the way of Miner's rule or (2):

$$SoD_M\ |_{HR\_Se} = \frac{m_k}{N_k} = \frac{n_k + m_{k-1@k}}{N_k} = \frac{n_k}{N_k} + \left(\frac{m_{k-1}}{N_{k-1}}\right)^{\frac{\log (s_k/s_e)}{\log (s_{k-1}/s_e)}}, \tag{13}$$

which can be written as

$$SoD_M\ |_{HR\_Se} = \left(\left(\left(\frac{n_1}{N_1}\right)^{\frac{\log (s_2/s_e)}{\log (s_1/s_e)}} + \frac{n_2}{N_2}\right)^{\frac{\log (s_3/s_e)}{\log (s_2/s_e)}} \cdots \frac{n_{k-1}}{N_{k-1}}\right)^{\frac{\log (s_k/s_e)}{\log (s_{k-1}/s_e)}} + \frac{n_k}{N_k}. \tag{14}$$

The SoD of HR-Se model also can be defined by the way of relative slope using the concept of the isolines of SoD as following:

$$SoD_S\ |_{HR\_Se} = \frac{\log\ (s_k/s_e)}{\log(m_k/N_e)} / \frac{\log\ (s_k/s_e)}{\log\ (N_k/N_e)} = \frac{\log\ (N_k/N_e)}{\log\ (m_k/N_e)}. \tag{15}$$

In this case, the relation between $SoD_S\ |_{HR\_Se}$ and $SoD_M\ |_{HR\_Se}$ can be expressed as:

$$SoD_S\ |_{HR\_Se} = \left(\frac{\log\ (SoD_M\ |_{HR\_Se})}{\log\ (N_k/N_e)} + 1\right)^{-1}. \tag{16}$$

C. STATE-OF-DAMAGE IN TS MODEL IN CASE OF HCF

It should be noted that the application of Miner's rule and HR models should be confined to addressing issues within High Cycle Fatigue (HCF), as these models rely on the S-N curve for life prediction. However, there has been a growing need to expand the applicability of CDMs to a broader range of scenarios, encompassing not only HCF but also Low Cycle Fatigue (LCF). To meet this demand, Golos and Ellyin introduced a novel CDM known as the Total Strain energy density (TS) model [23], [24], [25]. Unlike other approaches, the TS model provides a more comprehensive framework for fatigue analysis that can be applied across various fatigue regimes by considering the phases of crack initiation and propagation throughout the fatigue life, as well as a strain energy-based life prediction model. This innovative model offers the potential to enhance the accuracy and versatility of fatigue life predictions in a broader range of engineering applications.

TABLE 2. Summary of SoDs defined in CDMs and LPM used.

CDM	Miner's rule	HR-Su model	HR-Se model	TS model for HCF
SoD_M	$\frac{m_k}{N_k}$	$\frac{m_k}{N_k}$	$\frac{m_k}{N_k}$	$\frac{m_k}{N_k}$
SoD_S	N/A	$\frac{\log m_k}{\log N_k}$	$\frac{\log(N_k/N_e)}{\log(m_k/N_e)}$	$\frac{\log(N_k/N_e)}{\log(m_k/N_e)}$
SoD_λ	N/A	$\left(\frac{\log m_k}{\log N_k}\right)^{\lambda_k}$	$\left(\frac{\log(N_k/N_e)}{\log(m_k/N_e)}\right)^{\lambda_k}$	$\left(\frac{\log(N_k/N_e)}{\log(m_k/N_e)}\right)^{\lambda_k}$
LPM for HCF	$\sigma = CN^{-\frac{1}{b}}$	$s = N^{-\frac{1}{b}}$	$s = N^{-\frac{1}{b}}$ with N_e	$U = N^{-\frac{1}{2b}}$ with N_e

In this study, the focus will be limited to the HCF. In case of HCF, the TS model exhibits the linear relationship between fatigue life (N) and normalized strain energy density ($U = W/W_u$) in log-log scale, as illustrated in Fig. 2 (d). The details of life prediction model for TS model are elaborated upon in Section VI with comparison to S-N curve. Similar to the HR-Se model, the mathematical representation of the isolines of SoD for the TS model for HCF can be expressed as follows:

$$\frac{\log m_{k-1@k} - \log N_e}{\log U_k - \log U_e} = \frac{\log m_{k-1} - \log N_e}{\log U_{k-1} - \log U_e}$$
$$\text{or } \frac{m_{k-1@k}}{N_e} = \left(\frac{m_{k-1}}{N_e}\right)^{\frac{\log(U_k/U_e)}{\log(U_{k-1}/U_e)}}, \tag{17}$$

which is also equivalent to (4) and (5) in the Miner's rule.

The SoD can be also defined in two ways within the TS model. First, by the way of Miner's rule or (2), it becomes:

$$SoD_M\,|_{TS} = \frac{m_k}{N_k} = \frac{n_k + m_{k-1@k}}{N_k} = \frac{n_k}{N_k} + \left(\frac{m_{k-1}}{N_{k-1}}\right)^{\frac{\log(U_k/U_e)}{\log(U_{k-1}/U_e)}}. \tag{18}$$

It can be expressed as

$$SoD_M\,|_{TS} = \left(\left(\left(\frac{n_1}{N_1}\right)^{\frac{\log(N_2/N_e)}{\log(N_1/N_e)}} + \frac{n_2}{N_2}\right)^{\frac{\log(N_3/N_e)}{\log(N_2/N_e)}} \cdots \frac{n_{k-1}}{N_{k-1}}\right)^{\frac{\log(N_k/N_e)}{\log(N_{k-1}/N_e)}} + \frac{n_k}{N_k} \tag{19}$$

It mirrors the original definition of CDM in Golos and Ellyin study [23].

The TS model for HCF problem shares the similar concept with the HR-Se model for the isoline of SoD. Therefore, the SoD of TS model also can be defined by the way of relative slope as follows:

$$SoD_S\,|_{TS} = \frac{\log(U_k/U_e)}{\log(m_k/N_e)} \Big/ \frac{\log(U_k/U_e)}{\log(N_k/N_e)} = \frac{\log(N_k/N_e)}{\log(m_k/N_e)}. \tag{20}$$

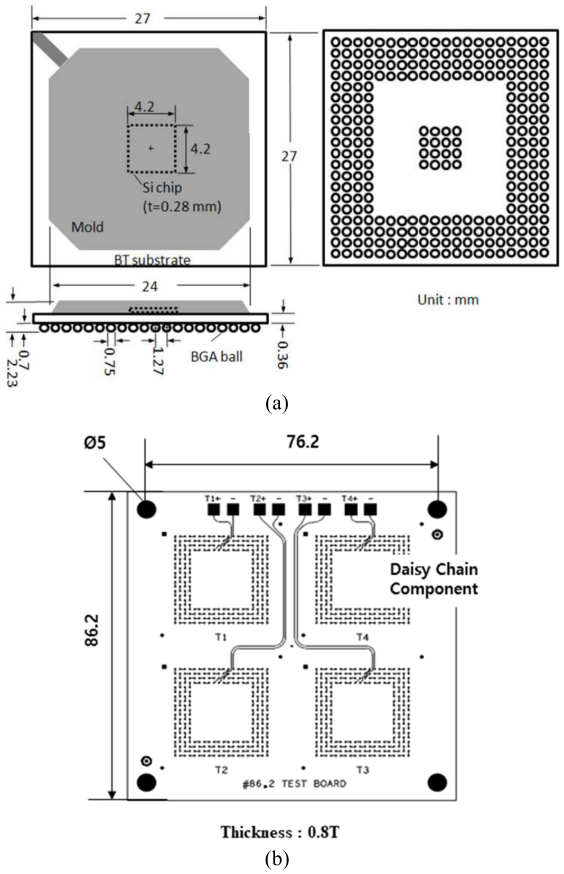

FIGURE 3. Diagram of (a) BGA package and (b) PCB design for experiment.

Note that this is the same with (15). Additionally, the relation between $SoD_S\,|_{TS}$ and $SoD_M\,|_{TS}$ is following:

$$SoD_S\,|_{TS} = \left(\frac{\log(SoD_M\,|_{TS})}{\log(N_k/N_e)} + 1\right)^{-1}. \tag{21}$$

The defined SoDs for the four CDMs are summarized in Table 2. The validation and challenges of the CDMs as well as the SoD definition for their implementation in PHM are discussed in the Section V. The fourth row in the table indicates a novel concept of SoD, which is presented in Section VI. The last row in the table indicates the adopted LPMs for the calculation CDMs, which is presented in the following Section.

IV. DEFINITION OF LIFE PREDICTION MODEL FOR CDM

To calculate the SoDs at each applied step of stress in variable loading, a LPM is required. For the purpose of this analysis, we considered the problem to be under HCF conditions and employed the S-N curve for LPM as follows:

$$\sigma = CN^{-\frac{1}{b}}, \tag{22}$$

where b and C are the fatigue strength exponent and material constant, respectively [26]. For the damage models for HR-Su

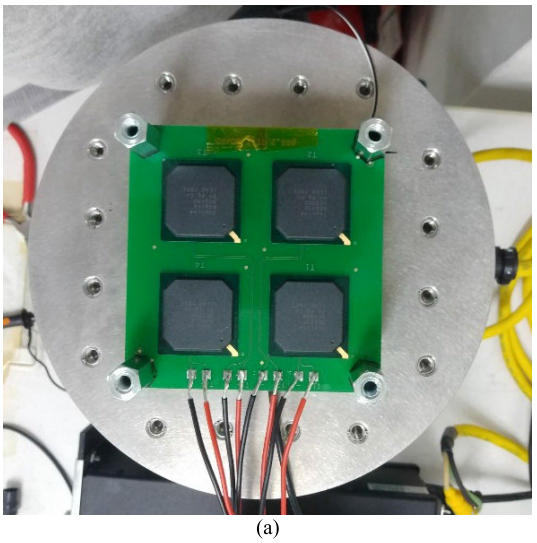
(a)

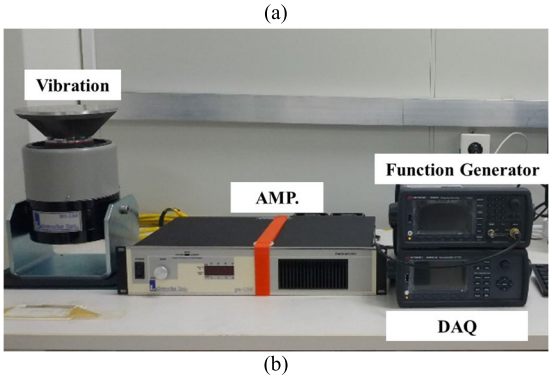

(b)

FIGURE 4. Experimental setup for the vibration test: (a) BGA packages connected by daisy chain and (b) experiment equipment.

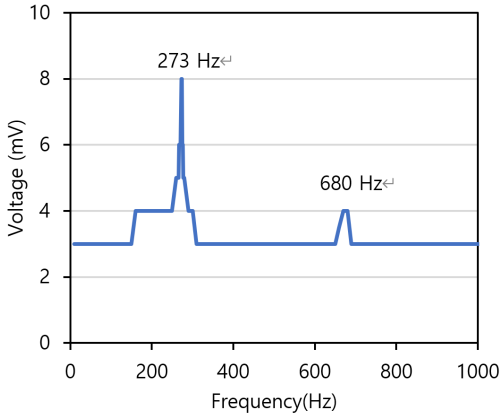

FIGURE 5. Experimental extraction of the first and second natural frequencies of the test coupon.

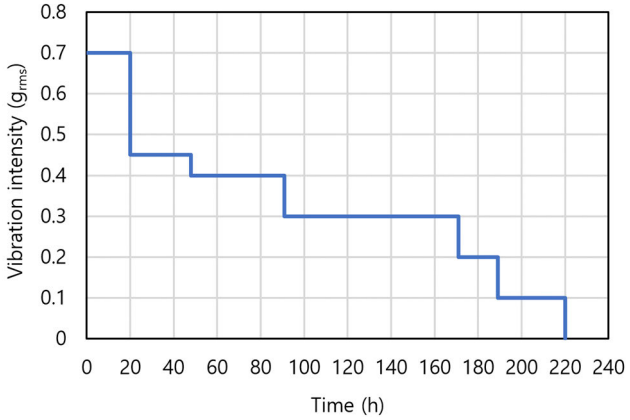

FIGURE 6. A field profile of vibration intensity at the pilot seat of a military helicopter for a year.

and HR-Se, equation (22) can be written in terms of the normalized stress, s, as

$$s = N^{-\frac{1}{b}}. \tag{23}$$

As discussed in Section III-C, the TS model was developed to broaden the applicability of CDMs to a wider range of scenarios, encompassing not only HCF but also LCF. The TS model defines the total strain energy density as follows [23]:

$$W = W^p + W^e = \frac{1-n^*}{1+n^*}\Delta\sigma^*\Delta\epsilon^p + (\Delta\sigma - \Delta\sigma^*)\Delta\epsilon^p + \frac{1}{2E}\left(\frac{1}{2}\Delta\sigma + \sigma_m\right)^2, \tag{24}$$

where W, W^p, and W^e are the total, elastic, and plastic strain energy density per cycle, respectively. Also, n^* is the cyclic strain-hardening exponent of master curve, $\Delta\sigma$ is the cyclic stress range, $\Delta\sigma^*$ is the cyclic stress range with origin at 0, σ_m is the mean stress, $\Delta\epsilon^p$ is the plastic components of strain range, and E is Young's modulus.

With the total strain energy density per cycle, the LPM becomes [23].

$$W = kN^c, \tag{25}$$

where k and c are the material parameters. When the plastic strain is negligible as in HCF problem and the mean value of stress is zero, after normalizing W to U, the LPM can be expressed as

$$U = \frac{W}{W_u} = \left(\frac{\sigma}{\sigma_u}\right)^2 = s^2 = N^c. \tag{26}$$

Utilizing (23), equation (26) can be estimated as

$$U = N^{-\frac{2}{b}}, \tag{27}$$

which is the LPM for TS model application. The summary of LPM is suggested in Table 2.

V. EXPERIMENTAL VALIDATION OF CDMs AND SoDs FOR PHM

Electronic circuit boards, typically composed of electronic components soldered onto Printed Circuit Boards (PCBs), are ubiquitous elements in electronic systems. Soldering is recognized as a significant wear-out mechanism in these board when subjected to thermal or vibrational environments [27], [28]. Numerous forecasts concerning future mobility indicate that vehicles will predominantly operate on roads rather than

TABLE 3. Applied profile of the vibration test with variable amplitude.

Step	Vibration intensity (g)	Exposed time (h)	No. cycles applied (n_k)	Step	Vibration intensity (g)	Exposed time (h)	No. cycles applied (n_k)
1	0.7	7	6,879,600	22	0.2	7	6,879,600
2	0.1	6	5,896,800	23	0.4	7	6,879,600
3	0.45	7	6,879,600	24	0.2	6	5,896,800
4	0.3	6	5,896,800	25	0.45	7	6,879,600
5	0.4	6	5,896,800	26	0.3	6	5,896,800
6	0.3	6	5,896,800	27	0.4	12	11,793,600
7	0.4	6	5,896,800	28	0.3	13	12,776,400
8	0.3	6	5,896,800	29	0.7	7	6,879,600
9	0.1	6	5,896,800	30	0.3	6	5,896,800
10	0.7	6	5,896,800	31	0.2	6	5,896,800
11	0.3	6	5,896,800	32	0.4	6	5,896,800
12	0.1	6	5,896,800	33	0.3	13	12,776,400
13	0.2	6	5,896,800	34	0.4	13	12,776,400
14	0.3	7	6,879,600	35	0.7	7	6,879,600
15	0.45	7	6,879,600	36	0.3	12	11,793,600
16	0.2	7	6,879,600	37	0.4	6	5,896,800
17	0.4	13	12,776,400	38	0.3	12	11,793,600
18	0.3	12	11,793,600	39	0.7	7	6,879,600
19	0.2	6	5,896,800	40	0.2	6	5,896,800
20	0.3	19	18,673,200	41	0.45	7	6,879,600
21	0.45	7	687,960	42	0.4	6	5,896,800

remain being parked [29], [30], consequently leading to an increased prevalence of vibrations as a potentially detrimental stress factor. In this study, the applicability of CDMs for PHM in electronics was assessed by investigating the solder's behavior under a variable vibration condition.

A. EXPERIMENT

To intensify the stress on the solder and streamline testing durations, a large electronic component or Ball Grid Array (BGA) package was selected. To gather a history of damage growth and failure data of solder in a variable vibration condition relevant to mobility, an electronic circuit board was designed. The board featured four BGA packages, each measuring 27 × 27 mm^2, positioned on an 86.2 × 86.2 mm^2 PCB as illustrated in Fig. 3. The solder used in the board was SAC305 (96.5% Sn, 3% Ag, 0.5% Cu), and each BGA package consisted of 256 solder joints. To monitor the fatigue life of the solder joints and confirm failures, the BGA packages were individually connected to four daisy chains, and real-time resistance measurement were conducted, as depicted in Fig. 4(a). To subject the board

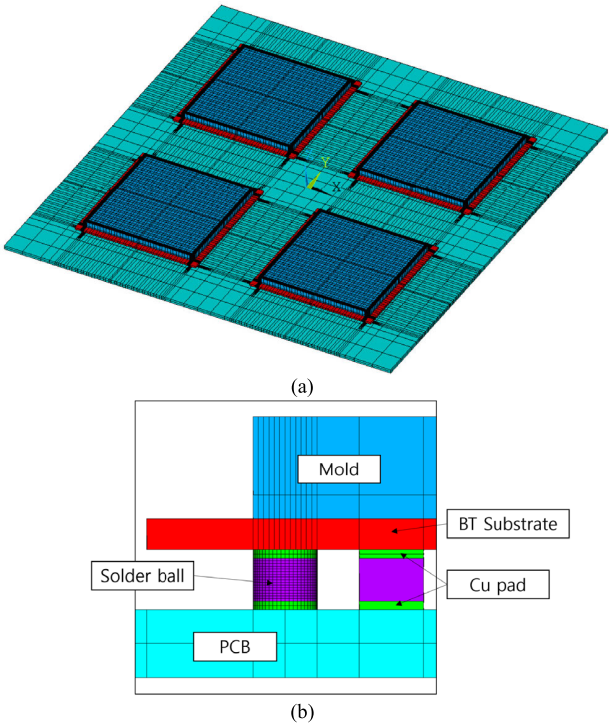

FIGURE 7. Finite element model of the BGA package; (a) isometric view and (b) side view on solder area in detail.

TABLE 4. Material properties used in the FEA model [35].

Component	Density (kg/m^3)	Elastic modulus (GPa)	Poisson's ratio
PCB	2,290	22	0.28
Solder	7,316	49	0.37
BT	1,910	22	0.39
Mold	2,000	20	0.3
Chip	2,330	112.4	0.28
Cu	8,953	120	0.33

TABLE 5. Relation between the vibration intensity, maximum stress on solder, and number of failure CYCL.

Intensity of vibration (g)	Maximum Von Mises stress on solder (MPa)	Number of failure cycle (N_k)
0.7	8.77	4.135E+07
0.45	5.64	6.204E+08
0.4	5.01	1.283E+09
0.3	3.76	7.464E+09
0.2	2.51	8.907E+10
0.1	1.25	6.415E+12

to a series of vibration conditions, a dedicated setup was employed, as shown in Fig. 4(b). The setup includes a shaker, an amplifier, and a function generator, generating a sinusoidal waveform on the board during the test process.

TABLE 6. Fatigue exponents of Solder SAC305 from references.

Ref.	b	Solder type	PCB size (LxW mm^2)	BGA package size (LxW mm^2)
Yu [31]	6.9	SAC 305	-	-
Xia [33]	8.7	SAC 305	200 × 56	14 × 14
Cinar [38]	2.1	SAC 305	133.4 × 30.0	11.0 × 7.5
Hauck [39]	8.1	SAC 305	-	-
Paquette [40]	4.8	SAC 305	-	-

Before conducting the vibration test, the natural frequency of the test board was determined by subjecting it to varying frequencies of vibration. The first natural frequency was recorded at 273 Hz, as illustrated in Fig. 5. The frequency was subsequently used for the frequency of the sinusoidal vibration test on the boards. In addition, the damping ratio of the board was determined using the half power bandwidth method [31], [32], [33], yielding a value of 0.016. This value was incorporated into the FE model of the board.

The intensity of the vibration test was determined based on a study for the vibration experienced by pilots in helicopters in the up-down direction [34]. This study identified a range of vibration intensities from 0.1 to 0.7 g. The duration of the vibration time was determined based on the operational schedule of a helicopter across a year [35]. The resulting vibration spectrum, which represents a practical field vibration profile for mobility applications, is presented in Fig. 6.

By employing a random selection from the vibration profile as summarized in Table 3, a tailored vibration test was devised and executed on the test board under its natural frequency. Note that the number of cycles applied in Table 3 was calculated by multiplying the natural frequency by the exposed time. During the vibration test, the resistance from the daisy-chained board was monitored every 0.2 seconds for each package. The failure of soldering was determined based on the criterion of a 20% increase in resistance observed consecutively for five times [36]. The vibration test was performed on two electronic circuit boards, resulting in failure times of 345 hours and 313 hours, respectively. The average lifetime of the boards was subsequently calculated to be 329 hours.

B. EXPERIMENT

The peak stress magnitude induced in the solder at each vibration level of the test was assessed using a commercial finite element package, ANSYS. The established finite element model, as depicted in Fig. 7, consists of PCB, solder ball, Si chip, BT substrate, package mold, and Cu pad. It has a total of 2,411,928 nodes, which was selected after a convergence study. The adopted material properties for the model are summarized in Table 4.

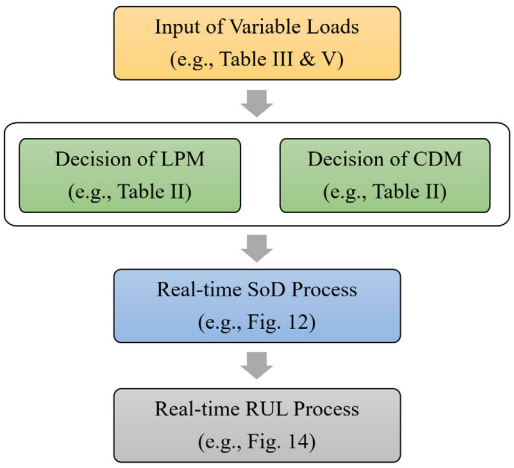

FIGURE 8. A PHM framework to process variable loading conditions.

The analysis under the tested vibration profile revealed that the vibration intensity of 0.7 g results in a peak stress of 8.77 MPa at the corner solder of BGA package. The summarized relation between the peak stress on the package and the vibration intensity on the board is presented in Table 5.

C. LIFE PREDICTION MODEL

In the applied vibration profile, the maximum stress (8.78 MPa) experienced by the solder in relation to its ultimate strength (49.5 MPa for SAC305 [37]) of solder equates to 18%, which is under the range of elastic strain or HCF. The value of exponent b in (22) was determined based on prior research. Several experimental studies [31], [33], [38], [39], [40], which conducted vibration tests on BGA packages under comparable conditions, yielded an average value of 6.12 as outlined in Table 6. It is worth noting for comparison that the typical value of b for SnPb solder is 4 [3]. The value of C was decided from the Steinberg assumption [3], where N is set to 10^3 when σ is the ultimate strength. In this context, equation (22) can be written as

$$\sigma = 149.76N^{-\frac{1}{6.12}}, \tag{28}$$

where the unit of stress is MPa. For the HR-Su and HR-Se models, equation (28) can be written in terms of the normalized stress, s, as

$$s = N^{-\frac{1}{6.12}}. \tag{29}$$

For the TS models, equation (27) can be written in terms of the normalized energy, U, as

$$U = N^{-\frac{1}{3.06}}. \tag{30}$$

The determination of the endurance limit (N_e) for the solder material is also essential to apply the CDMs of Table 2 to the experimental results. It demands a lot of time and financial resources, and the available studies on the data are limited. However, certain guidelines regarding on the

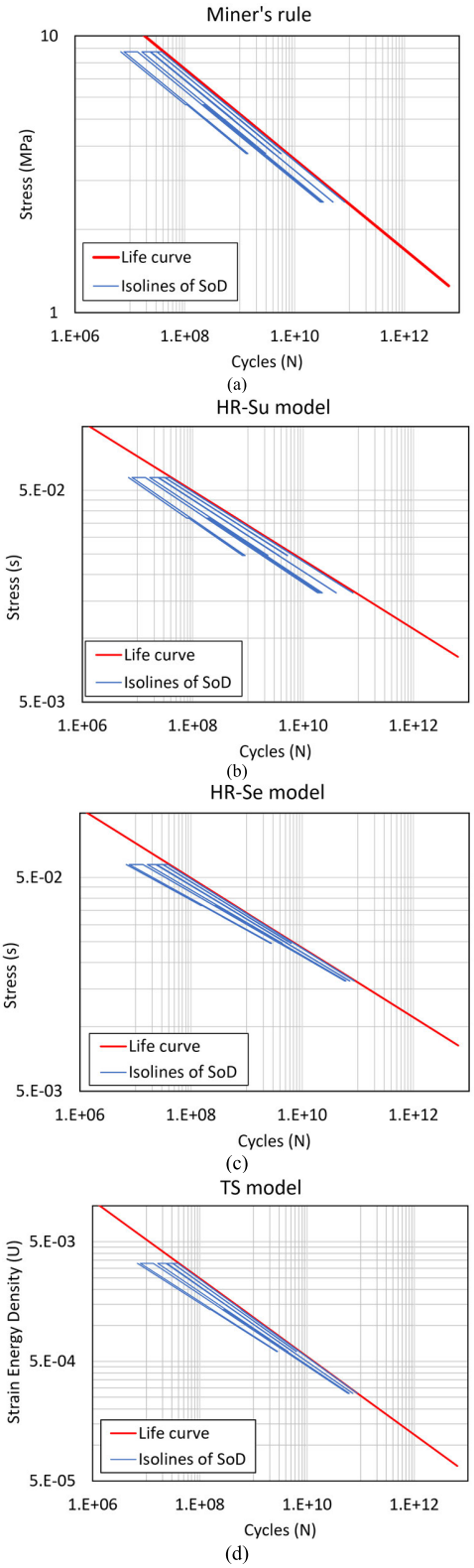

FIGURE 9. Growth of SoD isolines under the variable vibration in (a) Miner's rule, (b) HR-Su model, (c) HR-Se model, and (d) TS model.

number of endurance limits can be established from our experiment. In Table 5, the numbers of failure cycles at the applied intensity of vibrations are inserted at the last column

TABLE 7. Summary of the SoDs at the failure time by various CDMs.

CDM	SoD_M at the failure time	SoD_λ at the failure time
Miner's rule	0.938	-
HR-Su model	0.927	0.925
HR-Se model	0.993	0.994
TS model	0.993	0.994

using (28). Given that the number of failure cycles at the maximum stress on the solder (8.77 MPa) is 4.135E+7, the minimum endurance limit should surpass this value, or we can conservatively assume it to be 1.0E+8. Moreover, considering the number of cycles at the lowest applied stress on the solder as 6.415E+12, the largest potential endurance limit could extend up to 1.0E+14. This is a substantially higher value compared to the typical endurance limit [41], [42]. Based on these observations, it can be inferred that the endurance limit of solder SAC305 should fall within the range of 1.0E+8 and 1.0E+14. A sensitivity study on the endurance limit was conducted and discussed at Section VIII, which indicates that the conclusion is not highly influenced by the specific value of the endurance limit. Therefore, for subsequent analysis, the intermediate endurance limit value of 1.0E+11 was employed. In this scenario, the stress resulting from the vibration intensity of 0.1 g remains below the endurance limit stress.

D. IMPLEMENTATION

The calculation of SoD for the solder joint experiment under variable vibration loading conditions was conducted. The process of SoD calculation is summarized in Fig. 8. First, the sequence of applied vibration intensity and number of cycles were computed from the experimental data in Table 3, and the vibration intensity was then transformed into stress using Table 5. Next, the data underwent processing through the LPM and CDM, which are represented at Table 2. The results yielded the extent of SoD, the progressions of which are described in Fig. 9. Within these figures, the isolines of SoD illustrate the growth of SoD over the number of cycles. As the load is applied, these isolines of SoD gradually converge toward the life curve, commonly indicating the onset of failure. As suggested in Fig. 2, the application of Miner's rule resulted in parallel isolines of SoD. The HR-Su model led to isolines converging towards the maximum stress, while the HR-Se and TS models generated isolines that converged towards the endurance limit.

At the onset of failure, the projected values of SoD_M are summarized at the Table 7. Miner's rule anticipated 0.938 of SoD_M, whereas the HR-Se and TS models exhibited a higher accuracy of 0.993 of SoD_M. Within the HCF range, the HR-Se and TS models are equivalent, resulting in the same numbers. The HR-Su model yielded a less favorable value of 0.927 of SoD_M. This outcome is not surprising considering that the

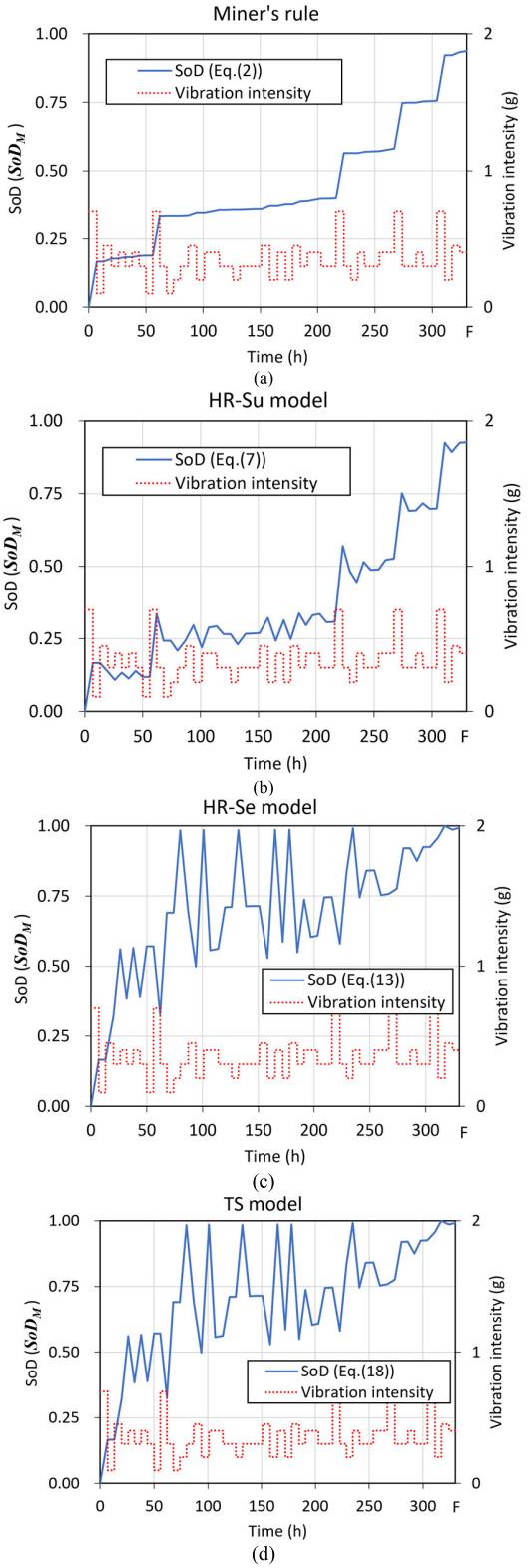

FIGURE 10. The change of SoD_M over time under the variable vibration in (a) Miner's rule, (b) HR-Su model, (c) HR-Se model, and (d) TS model.

HR-Su model is designed for the application in fatigue with a higher stress range compared to the HR-Se, as it converges at the ultimate strength.

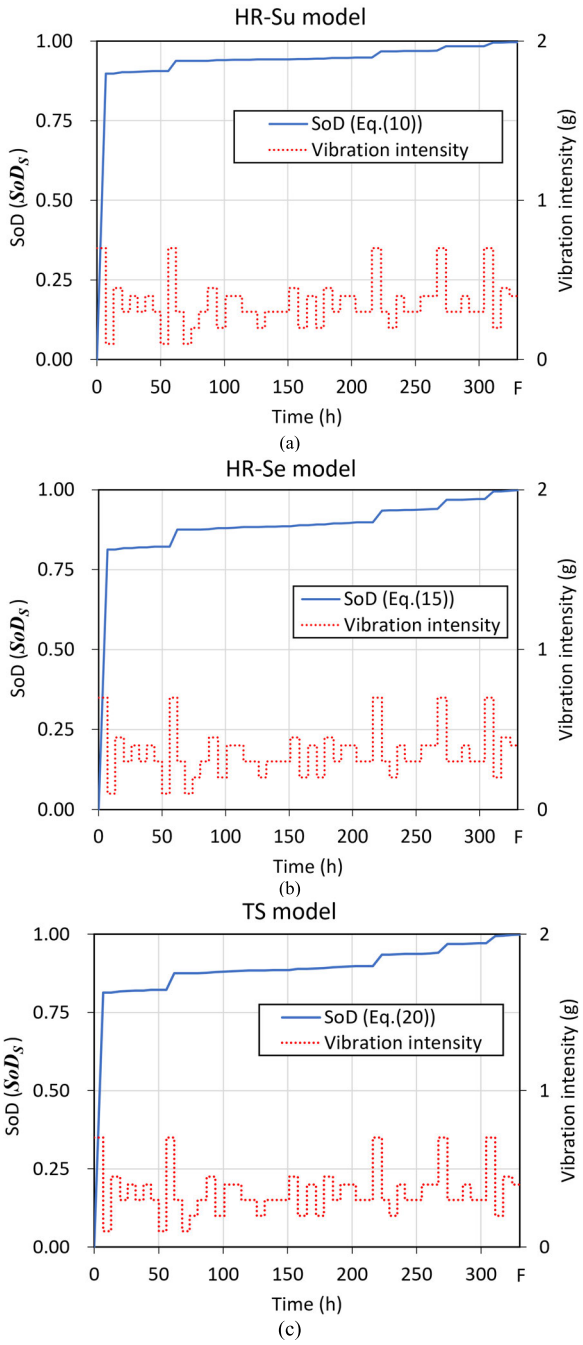

FIGURE 11. The change of SoD_M over time under the variable vibration in a) HR-Su model, (b) HR-Se model, and (c) TS model.

Based on the analysis, it becomes evident that the HR-Se and TS models outperform the Miner's rule in predicting failure, a finding consistent with prior research [22], [24]. However, when shifting the focus to the intermediate period leading up to failure, which is a point of interest in PHM, the results are not as straightforward as can be seen in Fig. 10. Figure 10 presents the trajectories of SoD_M in Miner's rule, HR models, and TS model.

In case of Miner's rule, the SoD_M consistently increases monotonically as indicated in Fig. 10(a), which is to be

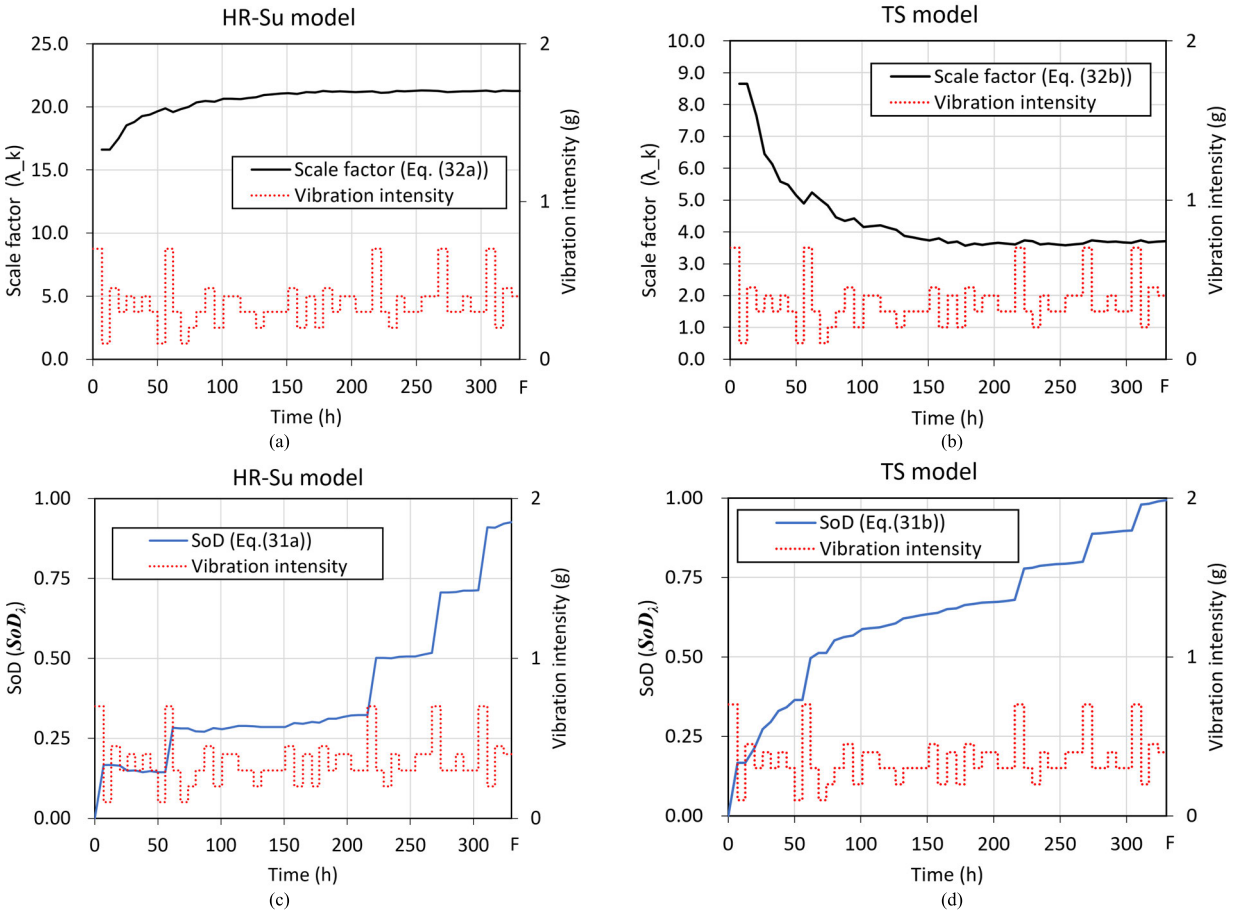

FIGURE 12. The change of scale factors defined by (32) and SoD_λ over time under the variable vibration in (a, c) HR-Su and (b, d) TS models.

expected from Fig. 9(a). However, in the cases of HR and TS models, the SoD_M experiences fluctuations as shown in Figs. 10(b) to (d). The fluctuation arises from that the isolines of SoD do not align parallelly with the LPM line, and the very definition of SoD_M allows for the possibility of inversion when observed on a linear scale. Furthermore, in the case of HR-Se and TS models, when the stress level is low, the m_k/N_k approaches 1. It elucidates the occurrence of three high peaks of SoD_M at low stresses prior to 200 h, as depicted in the Figs. 10 (c) and (d).

In PHM framework, the real-time monitoring of high peaks of SoD can lead to an incorrect indication of failure at early stages. For an accurate representation of physical damage in the structure, SoD should follow a monotonically increasing trend, accumulating along the applied stress. Therefore, the definition of SoD through SoD_M is unsuitable for implementation within the context of PHM.

By employing the definition of SoD_S instead of SoD_M, it becomes evident that the former exhibits a monotonically increasing trend for both HR and TS models, as depicted in Fig. 11. However, it is notable that they experience an exponential increase over 80% during the initial stage, which is not appropriate for the implementation in PHM framework. The reason for the exponential behavior is also a result of the definition itself. In the upcoming Section, a new definition of SoD was proposed, aimed at being suitable for PHM implementation.

VI. SoD WITH SCALE FACTOR

To address the problems but also adopting the advantages present in the definition of SoD, as depicted in the in Figs. 10 (linear but fluctuating) and 11 (monotonic but exponential), a novel definition of SoD incorporating a scale factor, λ, is introduced as follows.

For the HR-Su model:

$$SoD_\lambda = \left(\frac{\log m_k}{\log N_k}\right)^{\lambda_k}. \tag{31a}$$

For the HR-Se and TS models:

$$SoD_\lambda = \left(\frac{\log\left(N_k/N_e\right)}{\log\left(m_k/N_e\right)}\right)^{\lambda_k}. \tag{31b}$$

In the equations, λ_k represents the scale factor at the load step k. The scale factor serves to regulate the extent of exponential behavior in the SoD_S over real-time monitoring. Its determination can be based on the advantageous aspect of SoD_M, which exhibits an average linear increase as follows.

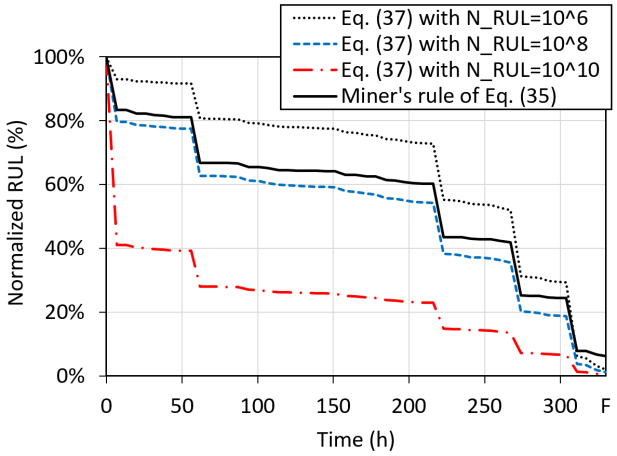

FIGURE 13. Change of normalized RULs under TS model with SoD_λ by the selection of the intended load level for the remaining lifespan (N_{RUL}) and comparison with the results of Miner's rule.

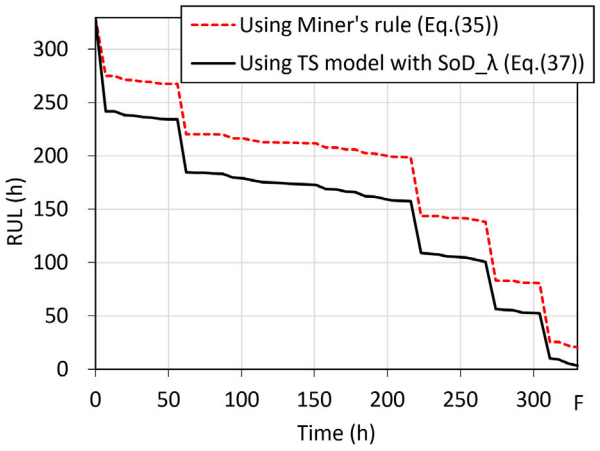

FIGURE 14. RUL predictions and comparisons for the Miner's rule and TS model with SoD_λ.

For the HR-Su model:

$$\lambda_k = \frac{1}{k}\sum_1^k \frac{\log\left(m_k/N_k\right)}{\log\left(\log m_k / \log N_k\right)}. \tag{32a}$$

For the HR-Se and TS models:

$$\lambda_k = \frac{1}{k}\sum_1^k \frac{\log\left(m_k/N_k\right)}{\log\left(\log\left(N_k/N_e\right)/\log\left(m_k/N_e\right)\right)}. \tag{32b}$$

Figure 12 displays the results of λ_k and SoD_λ obtained from the solder joint experiment under variable vibration in the previous Section, utilizing HR-Su and TS models. Notably, the scale factors converge to specific values rapidly as the load steps increase for both models. The behavior of SoD_λ, apart from the period during which λ_k is converging, demonstrates a monotonical increases without displaying exponential behavior. By combining the strengths of SoD_M and SoD_S, SoD_λ stands as a promising candidate for implementation within the PHM framework.

When examining the SoD_λ values at the points of failure, the TS model (0.994) once again demonstrates a higher accuracy in predicting failures compared to the HR-Su model (0.925), as outlined in Table 7. Furthermore, considering its potential for implementation beyond HCF, the PHM strategy for variable loading will choose to employ SoD_λ in conjunction with the TS model.

VII. RUL CALCULATION FROM SoD

When integrated into the PHM framework, the SoD can furnish real-time diagnostic information or the extent of current degradation of the system to the customers. However, the SoD offers qualitative information and does not deliver quantitative prognostic insight. To obtain a quantitative prognostic information, RUL is needed on a time scale, which can be defined in this study as:

$$RUL = \frac{n_{RUL}}{f_1}, \tag{33}$$

where n_{RUL} is the remaining number of cycles to failure at an intended stress level for the remaining lifespan, and f_1 is the first natural frequency of the system which will convert the cycles in n_{RUL} into a time scale.

For Miner's rule, RUL can be determined by setting SoD_M equal to 1 in (2) as in the following expression:

$$1 = \frac{n_{RUL}}{N_{RUL}} + \frac{m_k}{N_k}. \tag{34}$$

Consequently, RUL can be expressed using the current SoD_M and N_{RUL} as

$$RUL(k) = \frac{N_{RUL}(k)}{f_1}\left(1 - SoD_M(k)\right), \tag{35}$$

where N_{RUL} is the number of failure cycles at an intended load level for the remaining lifespan. Equation (35), if normalized by $N_{\mathrm{RUL}}(k)/f_1$, is the function of SoD_M only.

For TS model, equation (31b) can derive the RUL relationship by setting SoD_λ to 1 as follows:

$$1 = \left(\frac{\log\left(N_{RUL}/N_e\right)}{\log\left(\frac{n_{RUL}}{N_e} + \left(\frac{m_k}{N_e}\right)^{\frac{\log\left(N_{RUL}/N_e\right)}{\log\left(N_k/N_e\right)}}\right)}\right)^{\lambda_k}. \tag{36}$$

Subsequently, RUL can be expressed using the current SoD_λ and N_{RUL} as

$$RUL\left(k\right) = \frac{N_{RUL}\left(k\right)}{f_1} \times \left(1 - \left(\frac{N_k}{N_e}\right)^{\left(SoD_\lambda(k)^{-\frac{1}{\lambda_k}} - 1\right)\frac{\log\left(N_{RUL}(k)/N_e\right)}{\log\left(N_k/N_e\right)}}\right). \tag{37}$$

In the case of TS model, the RUL, if normalized by $N_{\mathrm{RUL}}(k)/f_1$, is a function of SoD_λ and N_{RUL}.

Equations (35) and (37), corresponding to RUL from Miner's rule and TS model, respectively, are compared in

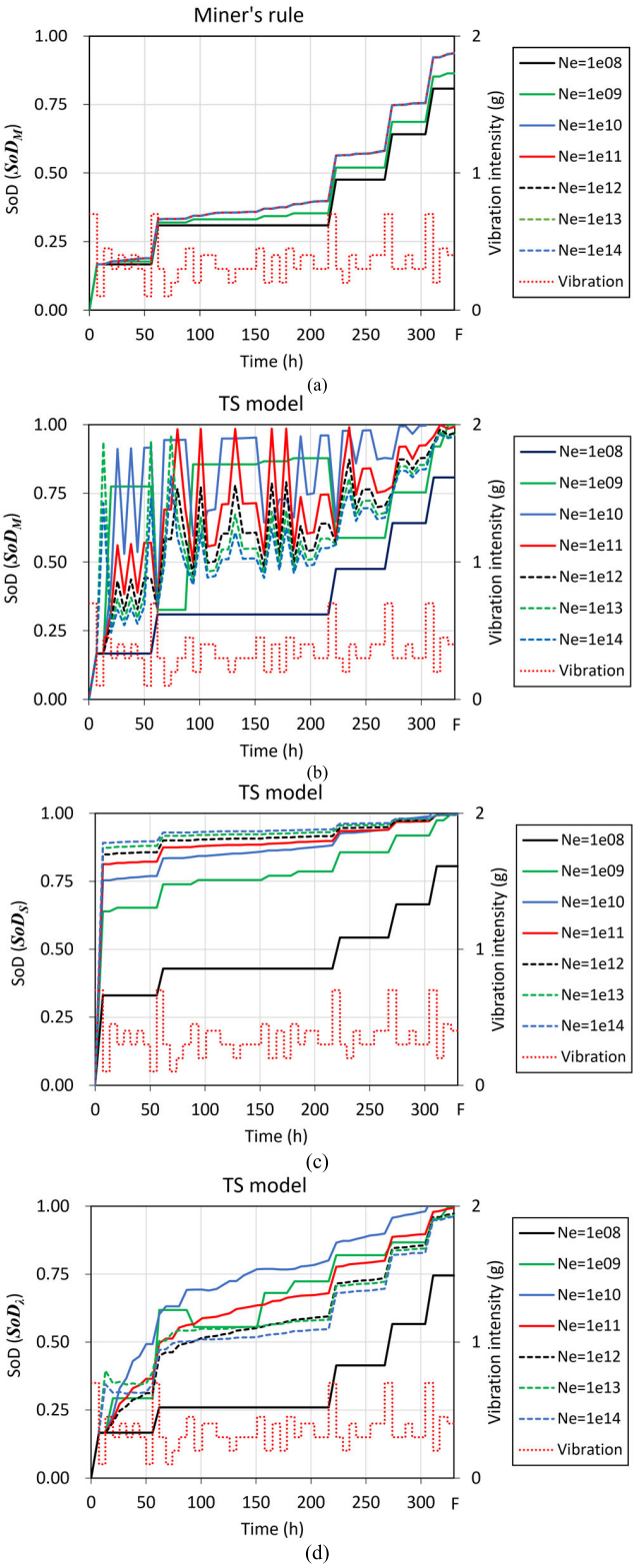

FIGURE 15. Sensitivity study results of the endurance limit (N_e) on (a) SoD_M in Miner' rules, (b) SoD_M, (c) SoD_S, and (d) SoD_λ in TS model.

Fig. 13 using the normalized scale. In the figure, it is evident that the normalized RUL derived from TS model with scale factor varies depending on the choice of N_{RUL}. This

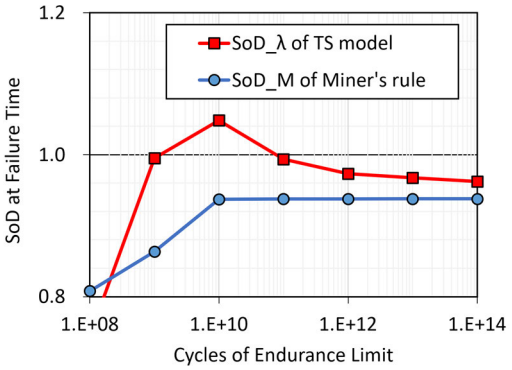

FIGURE 16. Sensitivity study results of the endurance limit (N_e) on SoDs at the failure time with SoD_M in Miner' rules and SoD_λ in TS model.

variability indicates the model's capacity to account for the effect of load sequence in RUL prediction. Conversely, this dependency is not observed in the case of the normalized RUL from Miner's rule.

If a planned usage is employed, predicting N_{RUL} becomes a feasible task. However, when random usage, such as in the mobility industry, is expected, it becomes challenging to anticipate an intended load level for the remaining lifespan. There could be various methods to predict future system usage by leveraging past usage patterns. But delving into these methods is beyond the scope of this study. Instead, for the purpose of this study, it was assumed that the lifetime has already been tested and is known for RUL prediction. In this case, N_{RUL} can be regarded as a constant value determined to align with the tested lifetime. It becomes $N_{\mathrm{RUL}} = 3.24\mathrm{E}{+}8$ for 330 h of lifetime and 273 Hz of the first natural frequency in this study.

With the number, the RULs are calculated from (35) and (37) and compared in Fig. 14. At the point of failure, the RULs predicted from (35) and (37) are 20.5 h and 3.2 h, respectively. These values correspond to 6.2 % and 1.0% of the total lifetimes, respectively. This analysis demonstrates that the TS models incorporating the SoD with the scale factor (SoD_λ) can predict RUL with better accuracy than Miner's rule.

VIII. DISCUSSION

In this Section, the impact of the endurance limit on the SoD results was discussed. The cycles of endurance limit (N_e) of the solder SAC305 was assumed as 1.0E+11 in this study. However, it can be ranged between 1.0E+8 and 1.0E+14, as considered in Section. V.C. When N_e changes from 1.0E+8 to 1.0E+14 in increments of 10, the SoD was assessed for both Miner's rule and TS model, and the outcomes are presented in Fig. 15.

First, the change of SoD_M of Miner's rule over time with the different values of N_e is illustrated in Fig. 15(a). The discrepancies among the cases can be attributed to the influence of the stress under the endurance limit, which becomes negligible. Consequently, the magnitude of SoD_M become

smaller as N_e decreases. Second, Figure 15(b) shows that the SoD_M of TS model fluctuates over time in regardless of N_e as seen from Fig. 10(d). But if N_e = 1.0E+8, there is no fluctuation in SoD_M since that only the highest stress of 8.77 MPa remained effective and the influence of variable loading becomes diminished in this case. Next, the SoD_S of TS model shows the trends of exponential increase over time in regardless of N_e as shown in Fig. 15(c). The increase of SoD_S magnitude as N_e increase can be again attributed to the influence of the stress under the endurance limit. The case of N_e = 1.0E+8 does not show the exponential increase by the same reason of the diminishing of variable loading influence. Finally, for the case of SoD_λ, there is no fluctuation of SoD as depicted in Fig. 15(b), and there is no exponential increase in Fig. 15(c) regardless of N_e. While there is difference among the cases of N_e, the overall trends of SoD_λ remain consistent, except the case of N_e = 1.0E+8 by the same reason as discussed in Figs. 15(a) to (c).

Furthermore, at the point of failure time, the SoD_λ of TS model was compared with SoD_M of Miner's rule across various N_e values as represented in Fig. 16. The SoD_λ of TS model exhibited better predictive accuracy for failure than Miner's rule across all N_e values except N_e = 1.0E+8. To sum up, it can be affirmed that the influence of the endurance limit on the SoD results is effectively minimized, and the choice of the endurance limit does not alter the conclusion that the TS models with SoD_λ can predict RUL with better accuracy compared to Miner's rule.

IX. CONCLUSION

This paper presented a comprehensive study on the application of CDMs for PHM in electronic systems, with a specific focus on solder joint reliability under variable vibration conditions. Various CDMs, including the TS model, were selected to address the limitations of Miner's rule. The SoD concept was introduced as a fundamental metric to evaluate PHM within each model. Through an extensive analysis, we evaluated the performance of these models in predicting failures and introduced a novel SoD definition that incorporates a scale factor. This innovative definition aimed to overcome the challenges posed by existing definitions, offering a promising compromise between linearity and exponential behavior within the context of PHM. Furthermore, the study demonstrates the calculation of RUL using the SoD metric and compares RUL predictions obtained from the conventional Miner's rule with those from the novel TS model incorporating the scale factor. The results highlight that the TS model, when enhanced with the scale factor, outperforms Miner's rule in accurately predicting SoD and RUL.

The introduction of a novel SoD definition along with the scale factor represents a potential breakthrough in overcoming the limitations of PHM application in electronics. As electronic systems continue to play an indispensable role across various industries, the insights derived from this study can contribute to improved reliability, performance, and operational efficiency through informed decision-making based on robust prognostic tools.

REFERENCES

[1] D. Beverungen, O. Müller, M. Matzner, J. Mendling, and J. V. Brocke, "Conceptualizing smart service systems," *Electron. Markets*, vol. 29, no. 1, pp. 7–18, Mar. 2019.
[2] D. Wanner, "Faults and their influence on the dynamic behaviour of electric vehicles," Ph.D. dissertation, KTH Royal Inst. Technol., Stockholm, Sweden, 2013.
[3] D. S. Steinberg, *Vibration Analysis for Electronic Equipment*. Hoboken, NJ, USA: Wiley, 2000.
[4] N. Kim, D. An, and J. Choi, *Prognostics and Health Management of Engineering Systems*. Berlin, Germany: Springer, 2017.
[5] A. K. M. Nor, S. R. Pedapati, and M. Muhammad, "Reliability engineering applications in electronic, software, nuclear and aerospace industries: A 20 year review (2000–2020)," *Ain Shams Eng. J.*, vol. 12, no. 3, pp. 3009–3019, Sep. 2021.
[6] C. Bhargava, P. K. Sharma, M. Senthilkumar, S. Padmanaban, V. K. Ramachandaramurthy, Z. Leonowicz, F. Blaabjerg, and M. Mitolo, "Review of health prognostics and condition monitoring of electronic components," *IEEE Access*, vol. 8, pp. 75163–75183, 2020.
[7] M. Pecht, "A PHM roadmap for electronics-rich systems," in *Prognostics and Health Management of Electronics: Fundamentals, Machine Learning, and the Internet of Things*. Hoboken, NJ, USA: Wiley, 2018.
[8] N. M. Vichare and M. G. Pecht, "Prognostics and health management of electronics," *IEEE Trans. Compon. Packag. Technol.*, vol. 29, no. 1, pp. 222–229, Mar. 2006.
[9] M. Pecht, "Prognostics and health monitoring of electronics," in *Proc. Int. Conf. Electron. Mater. Packag.*, Dec. 2007, pp. 1–8.
[10] Z. Wei, T. Junyong, and Z. Shufeng, "A life prediction method for electronic equipment under combined thermal cycling and vibration loading conditions," in *Proc. Prognostics Syst. Health Manage. Conf. (PHM-Hunan)*, Aug. 2014, pp. 11–15.
[11] A. Hanif, Y. Yu, D. DeVoto, and F. Khan, "A comprehensive review toward the state-of-the-art in failure and lifetime predictions of power electronic devices," *IEEE Trans. Power Electron.*, vol. 34, no. 5, pp. 4729–4746, May 2019.
[12] J. Gu, D. Barker, and M. Pecht, "Health monitoring and prognostics of electronics subject to vibration load conditions," *IEEE Sensors J.*, vol. 9, no. 11, pp. 1479–1485, Nov. 2009.
[13] L. Yang, L. Yin, B. Arafei, B. Roggeman, and P. Borgesen, "On the assessment of the life of SnAgCu solder joints in cycling with varying amplitudes," *IEEE Trans. Compon., Packag., Manuf. Technol.*, vol. 3, no. 3, pp. 430–440, Mar. 2013.
[14] J. Gu, D. Barker, and M. Pecht, "Prognostics implementation of electronics under vibration loading," *Microelectron. Rel.*, vol. 47, no. 12, pp. 1849–1856, Dec. 2007.
[15] K. Hectors and W. De Waele, "Cumulative damage and life prediction models for high-cycle fatigue of metals: A review," *Metals*, vol. 11, no. 2, p. 204, Jan. 2021.
[16] A. Fatemi and L. Yang, "Cumulative fatigue damage and life prediction theories: A survey of the state of the art for homogeneous materials," *Int. J. Fatigue*, vol. 20, no. 1, pp. 9–34, Jan. 1998.
[17] E. Santecchia, A. M. S. Hamouda, F. Musharavati, E. Zalnezhad, M. Cabibbo, M. El Mehtedi, and S. Spigarelli, "A review on fatigue life prediction methods for metals," *Adv. Mater. Sci. Eng.*, vol. 2016, Sep. 2016, Art. no. 9573524.
[18] K. J. Miller, "THE SHORT CRACK PROBLEM," *Fatigue Fract. Eng. Mater. Struct.*, vol. 5, no. 3, pp. 223–232, Jul. 1982.
[19] S. Subramanyan, "A cumulative damage rule based on the knee point of the S-N curve," *J. Eng. Mater. Technol.*, vol. 98, no. 4, pp. 316–321, Oct. 1976.
[20] M. A. Miner, "Cumulative damage in fatigue," *J. Appl. Mech.*, vol. 12, pp. 159–164, Jan. 1945.
[21] Z. Hashin, "A reinterpretation of the Palmgren-miner rule for fatigue life prediction," *J. Appl. Mech.*, vol. 47, no. 2, pp. 324–328, Jun. 1980.
[22] Z. Hashin and A. Rotem, "A cumulative damage theory of fatigue failure," *Mater. Sci. Eng.*, vol. 34, no. 2, pp. 147–160, Jul. 1978.
[23] K. Golos and F. Ellyin, "A total strain energy density theory for cumulative fatigue damage," *J. Pressure Vessel Technol.*, vol. 110, no. 1, pp. 36–41, Feb. 1988.

[24] K. Golos and F. Ellyin, "Generalization of cumulative damage criterion to multilevel cyclic loading," *Theor. Appl. Fract. Mech.*, vol. 7, no. 3, pp. 169–176, Jun. 1987.
[25] D. Kujawski and F. Ellyin, "A cumulative damage theory for fatigue crack initiation and propagation," *Int. J. Fatigue*, vol. 6, no. 2, pp. 83–88, Apr. 1984.
[26] O. H. Basquin, "The experimental law of endurance tests," *Proc. Amer. Soc. Test Mater.*, vol. 10, pp. 625–630, 1910.
[27] M. Thoben, F. Sauerland, K. Mainka, S. Edenharter, and L. Beaurenaut, "Lifetime modeling and simulation of power modules for hybrid electrical/electrical vehicles," *Microelectron. Rel.*, vol. 54, nos. 9–10, pp. 1806–1812, Sep. 2014.
[28] Y. Chen, B. Jing, J. Li, X. Jiao, J. Hu, and Y. Wang, "Failure analysis and modeling of solder joints in BGA packaged electronic chips," *IEEE Trans. Compon., Packag., Manuf. Technol.*, vol. 11, no. 1, pp. 43–50, Jan. 2021.
[29] R. Mounce and J. D. Nelson, "On the potential for one-way electric vehicle car-sharing in future mobility systems," *Transp. Res. A, Policy Pract.*, vol. 120, pp. 17–30, Feb. 2019.
[30] T. Litman. (2017). *Autonomous Vehicle Implementation Predictions*. Victoria Transport Policy Institute. [Online]. Available: https://www.vtpi.org/avip.pdf
[31] D. Yu, A. Al-Yafawi, T. T. Nguyen, S. Park, and S. Chung, "High-cycle fatigue life prediction for pb-free BGA under random vibration loading," *Microelectron. Rel.*, vol. 51, no. 3, pp. 649–656, Mar. 2011.
[32] J. Jang, G. Jang, J. Lee, Y. Cho, and Y. Cinar, "Fatigue life estimations of solid-state drives with dummy solder balls under vibration," *Int. J. Fatigue*, vol. 88, pp. 42–48, Jul. 2016.
[33] J. Xia, G. Li, B. Li, L. Cheng, and B. Zhou, "Fatigue life prediction of package-on-package stacking assembly under random vibration loading," *Microelectron. Rel.*, vol. 71, pp. 111–118, Apr. 2017.
[34] J. I. Kasin, N. Mansfield, and A. Wagstaff, "Whole body vibration in helicopters: Risk assessment in relation to low back pain," *Aviation, Space, Environ. Med.*, vol. 82, no. 8, pp. 790–796, Aug. 2011.
[35] S. Park and C. Han, "Design of accelerated life test in variable loading for military electronic system," in *Proc. Korean Soc. Mech. Engineers Annu. Fall Conf.*, 2020, pp. 1071–1076.
[36] *Performance Test Methods and Qualification Requirements for Surface Mount Solder Attachments*, Standard IPC-9701, IPC-Association Connecting Electronics Industries, 2002.
[37] *Indium Corp. Indalloy 256 96.5Sn/3.0Ag/0.5Cu Lead-Free Solder Alloy*. Accessed: Jan. 2, 2024. [Online]. Available: http://www.matweb.com/search/DataSheet.aspx?MatGUID=b1d03850d9854c24b25226694c6beed2
[38] Y. Cinar and G. Jang, "Fatigue life estimation of FBGA memory device under vibration," *J. Mech. Sci. Technol.*, vol. 28, no. 1, pp. 107–114, Jan. 2014.
[39] T. Hauck and I. Schmadlak, "Vibration durability of board mounted BallGridArrays," in *Proc. 14th Int. Conf. Thermal, Mech. Multi-Physics Simul. Experiments Microelectron. Microsystems (EuroSimE)*, Apr. 2013, pp. 1–4.
[40] B. M. Paquette, "Harmonic vibration testing of electronic components attached to printed wiring boards with SAC305 and eutectic SnPb solder," Ph.D. dissertation, Dept. Mech. Eng., Univ. Maryland, College Park, MD, USA, 2010.
[41] H. S. Blanks, "Accelerated vibration fatigue life testing of leads and soldered joints," *Microelectron. Reliab.*, vol. 15, no. 3, pp. 213–219, 1976.
[42] J. Thambi, U. Tetzlaff, A. Schiessl, K.-D. Lang, and M. Waltz, "High cycle fatigue behaviour and generalized fatigue model development of lead-free solder alloy based on local stress approach," *Microelectron. Rel.*, vol. 66, pp. 98–105, Nov. 2016.

SUYEON LEE received the B.S. and M.S. degrees in mechanical engineering from The State University of New York, Korea (SUNY Korea), Incheon, South Korea, in 2020 and 2022, respectively. From 2020 to 2023, she was a Research Assistant with the Physics-of-Failure Laboratory, SUNY Korea. In 2023, she joined the National Cancer Center, Ilsan-ro, South Korea, as a Researcher. Her current research interests include reliability, prognostics and health management, electronics, and designing in orthopedic biomechanics.

SEUNGIL PARK received the B.S. degree in electronic engineering from the Tech University of Korea, Gyeonggi-do, South Korea, in 2012, the M.S. degree from Hanyang University, Seoul, South Korea, in 2015, and the M.S. degree in mechanical engineering from The State University of New York, Korea (SUNY Korea), Incheon, South Korea. From 2013 to 2017, he was a Researcher with the Korea Electronics Technology Institute. Since 2023, he has been a Research Assistant with the Department of Mechanical Engineering, SUNY Korea. His research interests include accelerated lifetime test and accelerated stress test design, lifetime improvement of electronic devices, modules, and systems, and physics-of-failure-based reliability.

CHANGWOON HAN received the B.Sc. and M.Sc. degrees in mechanical engineering from Seoul National University, Seoul, Republic of Korea, in 1993 and 1995, respectively, and the Ph.D. degree in mechanical engineering from the University of Maryland, College Park, MD, USA, in 2005. He was a Principal Research Engineer with the Korea Electronics Technology Institute, Seongnam-si, Republic of Korea, from 2005 to 2017. He is currently an Associate Professor with the Department of Mechanical Engineering, The State University of New York, Korea, Incheon, Republic of Korea. His research interests include physics-of-failure, prognostics and health management, design-for-reliability, and photomechanics.